© 2018. Published by The Company of Biologists Ltd | Journal of Experimental Biology (2018) 221, jeb163360. doi:10.1242/jeb.163360

RESEARCH ARTICLE

The relationship between pectoral fin ray stiffness and swimming behavior in Labridae: insights into design, performance and ecology

Brett R. Aiello[1,*], Adam R. Hardy[1], Chery Cherian[2], Aaron M. Olsen[1], Sihyun E. Ahn[2], Melina E. Hale[1] and Mark W. Westneat[1,*]

ABSTRACT

The functional capabilities of flexible, propulsive appendages are directly influenced by their mechanical properties. The fins of fishes have undergone extraordinary evolutionary diversification in structure and function, which raises questions of how fin mechanics relate to swimming behavior. In the fish family Labridae, pectoral fin swimming behavior ranges from rowing to flapping. Rowers are more maneuverable than flappers, but flappers generate greater thrust at high speeds and achieve greater mechanical efficiency at all speeds. Interspecific differences in hydrodynamic capability are largely dependent on fin kinematics and deformation, and are expected to correlate with fin stiffness. Here we examine fin ray stiffness in two closely related species that employ divergent swimming behaviors, the flapping *Gomphosus varius* and the rowing *Halichoeres bivittatus*. To determine the spatial distribution of flexural stiffness across the fin, we performed three-point bending tests at the center of the proximal, middle and distal regions of four equally spaced fin rays. Pectoral fin ray flexural stiffness ranged from 0.0001 to 1.5109 μN m^2, and the proximal regions of *G. varius* fin rays were nearly an order of magnitude stiffer than those of *H. bivittatus*. In both species, fin ray flexural stiffness decreased exponentially along the proximodistal span of fin rays, and flexural stiffness decreased along the fin chord from the leading to the trailing edge. Furthermore, the proportion of fin area occupied by fin rays was significantly greater in *G. varius* than in *H. bivittatus*, suggesting that the proportion of fin ray to fin area contributes to differences in fin mechanics.

KEY WORDS: Wrasse, Flexural stiffness, Mechanics, Locomotion, Propulsion

INTRODUCTION

The form and function of propulsive appendages are fundamental to the ecology of a wide range of organisms (Liem, 1990; Losos, 1990; Wainwright and Reilly, 1994; Gillis and Blob, 2001; Taft and Taft, 2012; Higham et al., 2015). In coral reef fishes, interspecific variation of fin form and function has a strong impact on hydrodynamic capability in fishes (Walker and Westneat, 2000, 2002a,b; Thorsen and Westneat, 2005), and has ultimately shaped patterns of niche occupation (Bellwood and Wainwright, 2001; Fulton et al., 2001; Wainwright et al., 2002). Daniel and Combes (2002) explored the flexural stiffness of insect wings, and suggested that because of the complex relationship existing between the form and function of a propulsor, predictions of functional capabilities in propulsors based on shape alone are valid only under limited circumstances. The mechanics of insect wings (Newman and Wootton, 1986; Ennos, 1988a; Steppan, 2000; Combes and Daniel, 2003a,b), bird wings (Macleod, 1980; Bonser and Purslow, 1995; Bachmann et al., 2012) and bat wings (Swartz et al., 1996; Swartz and Middleton, 2008) share characteristics of their stiffness fields (the spatial distribution of flexural stiffness across an appendage), including a stiffened leading edge, a more flexible trailing edge, and a structure that tapers along its span. Together, these common features of stiffness profiles lead to the convergence of similar propulsor bending regimes across a highly diverse group of taxa (Lucas et al., 2014). Yet, fin ray stiffness is rarely considered in the discussion of fin design and hydrodynamic capability in fishes; this leads to questions of how the distribution of mechanical properties across the fins of fish relates to swimming behavior, whether the distribution of fin mechanics leads to the passive production of an advantageous bending regime across the surface of a fin, and how pectoral fin mechanics compare with the mechanics of flexible propulsors found in other systems. Our understanding of fish fin biomechanics, hydrodynamic capability and evolutionary diversification may thus benefit through efforts to document associated variation in the mechanical properties of the fin.

The pectoral fin is a flexible propulsor with a composite structure typically composed of a membrane supported by multiple fin rays (Goodrich, 1904). Fin rays, or lepidotrichia, are bilaminar composite structures made up of two crescent-shaped acellular bony hemitrichia (Geerlink and Videler, 1987) that surround a core of collagen gel (Goodrich, 1904). In pelagic fishes, the proximal portion of each hemitrich is typically unsegmented and the distal portion is segmented (Goodrich, 1904). Up to four muscles attached via tendons to the proximal base of each fin ray control the movement of individual rays, as well as the fin as a whole (Geerlink and Videler, 1987; Lauder et al., 2011). Although many animals (e.g. birds, bats and fishes) are capable of actively tuning the shape or mechanics of their flexible propulsor (Geerlink and Videler, 1987; Kent and Carr, 2001; Lauder et al., 2006; Alben et al., 2007; Cheney et al., 2014), the flexural stiffness of a structure, or its resistance to bending, will largely determine its shape change in response to the application of locomotor forces (Gordon, 1978; Vogel, 2003). The propulsive and maneuverability capabilities of animals with flexible propulsors are largely dependent on the kinematics and three-dimensional deformation of their appendages (Yamamoto et al., 1995; Daniel and Combes, 2002; Zhu and Shoele, 2008; Young et al., 2009; Tangorra et al., 2010; Flammang

[1]Department of Organismal Biology and Anatomy, University of Chicago, Chicago, IL 60637, USA. [2]The College, University of Chicago, Chicago, IL 60637, USA.

*Authors for correspondence (mwestneat@uchicago.edu; braiello@uchicago.edu)

B.R.A., 0000-0001-9034-0460; A.R.H., 0000-0003-3370-7144; M.E.H., 0000-0001-5194-1220; M.W.W., 0000-0002-3548-7002

Received 22 May 2017; Accepted 13 November 2017

et al., 2013; Mistick et al., 2016). Therefore the deformation of the pectoral fin surface in fishes performing labriform locomotion will be significantly affected by the spatial distribution of spanwise (along the length of the fin from proximal to distal) and chordwise (across the width of the fin from its leading edge to the trailing edge) fin ray flexural stiffness, and the distribution of stiffness across the fin could be tuned to differences in hydrodynamic performance and capable of passively producing advantageous deformations.

The spatial distribution of intrinsic pectoral fin ray flexural stiffness has been explored in the bluegill sunfish (*Lepomis macrochirus*) (Tangorra et al., 2010; Lauder et al., 2011; Flammang et al., 2013). In the bluegill pectoral fin, the stiffness of a given ray decreases from proximal to distal, and, across the chord, the central rays are stiffer than the dorsal and ventral rays (Tangorra et al., 2010; Lauder et al., 2011). Beyond bluegill, our understanding of fin ray stiffness is inferred from differences in fin ray geometry in specialized benthic species (Taft, 2011; Taft and Taft, 2012). Aiello et al. (2017) also reported the comparative stiffness of a single ray in eight labrid species and found that flexural stiffness decreased exponentially along the length of the third fin ray in all species, and that fin ray stiffness was related to swimming behavior. The third pectoral fin ray was significantly stiffer in labrid species that employed the flapping swimming behavior in comparison with species that employed rowing swimming behavior (Aiello et al., 2017). A larger body of comparative work on fin stiffness is necessary to address questions regarding the features of pectoral fin ray stiffness that are general to actinopterygians, how the spatial distribution of flexural stiffness across a fin varies among species, and associations among pectoral fin stiffness profile, swimming behavior, hydrodynamic capability and the ecology of fishes. Differences in swimming behavior and trade-offs between maneuverability and propulsive efficiency would be expected to drive the evolution of different pectoral fin flexural stiffness spatial profiles among species.

Here we explore these questions in the wrasses (Labridae), a clade that employs pectoral fin-based propulsion with kinematics ranging from drag-based rowing to lift-based flapping (Walker and Westneat, 2000, 2002a,b). Rowers generate thrust primarily during their posteriorly directed power stroke, generate greater thrust at slow speeds, and are more maneuverable in comparison with flappers (Walker and Westneat, 2000, 2002a,b). Conversely, flappers generate thrust during both the upstroke and downstroke, and generate greater thrust at high speeds and greater mechanical efficiency at all speeds in comparison with rowers (Walker and Westneat, 2000, 2002a,b). Although a flexible propulsor will typically generate more thrust in comparison with a rigid propulsor (Yamamoto et al., 1995; Zhu and Shoele, 2008; Young et al., 2009), excessive flexibility reduces propulsive efficiency (Liu and Bose, 1997; Heathcote et al., 2008). In addition, modelling studies have found that a biorobotic fin with stiff and tapered fin rays exhibits greater propulsive capabilities than a fin with relatively more flexible and uniformly designed rays (Tangorra et al., 2010). Therefore we hypothesized that fin ray stiffness would decrease along the span of the fin ray from proximal to distal in both flappers and rowers, and flappers would have stiffer fins in comparison with rowers, which might allow flappers increased efficiency and rowers increased maneuverability.

To address these hypotheses we assessed pectoral fin ray flexural stiffness in two closely related and size-matched species, the flapping *Gomphosus varius* and the rowing *Halichoeres bivittatus*. Here we assess passive flexural stiffness, which is not influenced by the active displacement or stabilization of opposing hemitrichs that is suggested to occur through the differential activity of antagonistic muscles (Alben et al., 2007). To determine the spatial distribution of flexural stiffness, we performed three-point bending tests at the center of the proximal, middle and distal third of four equally spaced fin rays across the chord of each fin. We compared the spatial distribution of *G. varius* and *H. bivittatus* pectoral fin flexural stiffness with published data from other species to begin to explore how different stiffness profiles relate to the swimming behavior, hydrodynamic capability and niche of a species. In addition, because fin shape (aspect ratio) is correlated with swimming behavior (Wainwright et al., 2002; Walker and Westneat, 2002b) and we have observed interspecific differences in the number of fin rays per fin, we also quantified the area of a fin covered by ray versus membrane to probe the morphological underpinning of variation in fin stiffness.

A comparative analysis of the spatial distribution of pectoral fin ray flexural stiffness and how it relates to fin morphology provides new insights into fin function and builds upon recent work (Tangorra et al., 2010; Lauder et al., 2011; Taft, 2011). In addition, this study broadens our understanding of the diversity of fin ray mechanical properties, providing a foundation for comparative and phylogenetic studies of pectoral fin function that include the mechanical properties of fin tissues.

MATERIALS AND METHODS

Fish specimens

We collected data on the mechanical properties of the pectoral fin rays from seven *Gomphosus varius* Lacépède 1801 individuals (mass ranged between 7.8 and 39.8 g; mean±s.d., 22.44±13.19 g) and eight *Halichoeres bivittatus* (Bloch 1791) individuals (mass ranged between 6.0 and 64.6 g; mean±s.d., 22.03±19.05 g). Fish were obtained commercially and maintained in 200 liter capacity marine aquaria (34.51 p.p.t.) under natural day:night light cycles with a mean water temperature of 24°C. Fish were killed by immersion in a 0.05 g l^{-1} solution of MS-222 (tricaine methanesulfonate; Sigma-Aldrich, St Louis, MO, USA), and the right pectoral fins were then excised from the body and placed in extracellular solution to maintain cell survival and structural integrity. All experimental treatments and procedures were carried out under University of Chicago Institutional Animal Care and Use Committee guidelines (protocol 72365 to M.W.W.).

Three-point bending tests

In order to determine the spatial distribution of intrinsic pectoral fin ray stiffness we performed three-point bending tests on the fin rays of *G. varius* and *H. bivittatus* using similar methods to Aiello et al. (2017), with an independent sample and testing protocol. We used a material testing machine (LS1; Lloyd Instruments, Fareham, UK) with a 10 N load cell (minimum load resolution 0.0001 N). Data were acquired during dynamic force displacement tests at 1000 Hz using Nexygen Plus software (Lloyd Instruments). The raw forces measured ranged between 0.0004 and 0.4325 N across all individuals and measurement locations. The potential error in force measurement across most of the force range was generally low (0.5–1%), but was higher (up to 12.5%) for the smallest trailing edge fin rays measured.

Flexural stiffness (*EI*) is a measurement of a structure's resistance to bending and depends upon its material properties (*E*, Young's modulus of elasticity) and cross-sectional geometry (*I*, second moment of area) (Gordon, 1978; Vogel, 2003). The conditions to measure *E* and *I* independently are rarely met for biological materials, as the material must be homogenous, isotropic and linearly elastic (Vogel, 2003; Young et al., 2012). Furthermore, fin

Journal of Experimental Biology (2018) 221, jeb163360. doi:10.1242/jeb.163360

rays are composite structures (i.e. crescent-shaped hemitrichia that surround a core of collagen gel), making accurate and reliable measurements of I difficult. Therefore, we measured EI as a single variable using beam theory as in Vogel (2003): $EI=(Fd^3)/(48Y)$, where F is applied force (N), d is the distance between supports (m), and Y is fin ray displacement (m) at the location of the force application (Fig. 1). Elastic non-linearity can still exist, even at small deformations, which could change the relative effective flexural stiffness of a structure at different bending amplitudes. The beam theory equation is widely used to investigate the flexural stiffness of biological structures (for a review, see Vogel, 2003), and provides an appropriate approximation of the flexural stiffness of a structure. This equation is valid for small displacements where $Y \leq 10\%$ of fin ray length (L) because a material can experience shear as well as bending at larger displacements (Blob and LaBarbera, 2001; Young et al., 2012). Therefore, we measured the force exerted when fin ray displacement (Y) ranged from 0 up to 10% of L. This corresponds to a bending curvature of 0.2–0.5 mm^{-1}, defined as the inverse radius of curvature of the circle defined by the partial circumference represented by the curved fin ray. This range of curvature is similar to that observed in the fin rays of live, actively swimming *G. varius* and *H. bivittatus*.

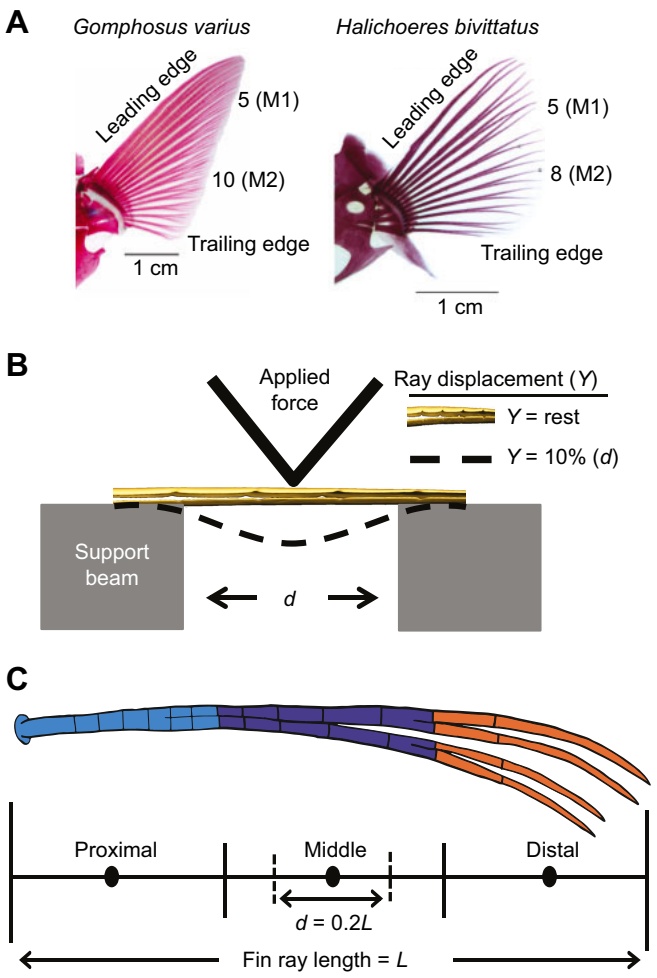

Fig. 1. Schematic diagram of the methodology used in this study. (A) The leading edge ray, trailing edge ray, and two middle fin rays (fin ray 5=M1 and fin ray 8 or 10=M2) equidistant from each other and from the leading and trailing rays were dissected from fresh fins and used for mechanical property testing. The fins pictured are cleared and stained versions for morphological reference. Y, fin ray displacement; d, distance. (B) Fin rays were isolated and placed on a three-point bending apparatus. (C) Individual tests were conducted at three different locations per fin ray: the middle of the proximal third (16.65% fin ray length), the middle of the middle third (50.00% fin ray length), and the middle of the distal third (83.34% fin ray length).

Pectoral fin rays 1 (leading edge), 5, 10 and 14 (trailing edge) of *G. varius* and 1, 5, 8 and 12 of *H. bivittatus* were individually dissected from the pectoral fin (Fig. 1A). Fin rays were placed across adjustable support beams so that flexural stiffness was measured at the center of the proximal (16.67% ray length), middle (50% ray length) and distal (83.25% ray length) third of each fin ray (Fig. 1). To standardize measurements across species, the distance between supports (d) was set to 20% of L, and force was applied at a rate of 0.1 mm s^{-1}. Fin rays were kept moist with 4°C phosphate-buffered saline solution throughout the duration of the experiment.

To ensure the most accurate measurement of fin ray flexural stiffness, local three-point bending tests were conducted at proximal, middle and distal locations along the length of the fin. The gradual change in fin ray cross-section that occurs locally within these small regions allows the three-point bending equation to be applied with sufficient accuracy (Young et al., 2012). Furthermore, in the proximal bending location, force was always applied to a section that was unsegmented. This method can accurately measure flexural stiffness at multiple locations along a single fin ray, and when done on multiple fin rays, can reveal the spatial distribution of flexural stiffness across a fin.

A single value of flexural stiffness per fin ray could be obtained by conducting cantilever-bending tests (Vogel, 2003). However, cantilever-bending tests have several assumptions that are not met by fin rays. Fin rays are continuously tapered structures. Although equations have been developed to deal with continuously tapered structures with varying success (Young et al., 2012), these methods require knowledge of the variation in second moment of area along the length of the beam. Attempts have been made to measure second moment of area in fin rays (Taft, 2011). However, the complex bilaminar structure of two independent hemitrichs surrounding a core of collagen and the unknown contributions of these materials to fin ray stiffness makes it difficult to accurately measure the second moment of area. Finally, fin rays are typically unsegmented proximally and segmented distally. Although equations have been developed to measure the flexural stiffness of slotted uniform beams during cantilever bending (Young et al., 2012), no equations exist, to the best of our knowledge, to account for a tapered beam that abruptly becomes segmented.

Heat maps of fin ray stiffness across the fin surface were produced by fitting a two-parameter linear model to the log10-transformed measured stiffness values for each individual using the R base function ‘lm’. The sampled locations correspond to the arithmetic mean stiffness measured at that point on the fin. These means values were calculated from the log10-transformed values, which were transformed back into the measured stiffness units for presentation in Fig. 2. All colors outside the black circles (including portions more proximal and distal to the sampled locations) were determined using the linear model fit and the R base function ‘predict’. The adjusted R-squared of the model fit to *G. varius* is 0.629 (residual standard error, in log10-transformed units: 0.4093) and the adjusted R-squared of the model fit to *H. bivittatus* is 0.796 (residual standard error, in log10-transformed units: 0.3712).

Skeletal area

We hypothesize that the thickness, branching and overall skeletal area of the fin rays within the fin blade is related to the overall fin stiffness. Therefore an additional goal of this study was to quantify

Journal of Experimental Biology (2018) 221, jeb163360. doi:10.1242/jeb.163360

the area of a fin occupied by ray skeleton in both species. We measured skeletal area: the percentage of fin surface area occupied by fin ray skeleton (as opposed to the area occupied by only fin membrane). For each species, five cleared and stained specimens were acquired from the Field Museum of Natural History (Chicago, IL, USA); *G. varius*: FMNH 124858, 111975, 111976 and 101280 (*N*=2); *H. bivittatus*: FMNH 101276 (*N*=2) and MW-NC92 (*N*=3). The fins were preserved, cleared and stained in standard splayed position following previous studies (Wainwright et al., 2002; Thorsen and Westneat, 2005). To ensure comparability between species, fins were preserved (10% buffered formalin) with the fins splayed to the point where the membrane is fully extended but not stretched beyond this point. The cleared and stained individuals of each species fell within the same size range of the experimental individuals used in this study. The length of the leading edge fin ray ranged between 1.269 and 2.953 cm in *G. varius* (mean±s.d., 2.146±0.619 cm) and 1.287 and 2.383 cm in *H. bivittatus* (mean±s.d., 2.036±0.438 cm). Leading edge fin ray length was not significantly different between species (P=0.754). Excised fins were placed on a white light board with fin rays in a splayed position. Digital images were captured using an Olympus DP72 camera (Olympus, Center Valley, PA, USA). Images were imported into Adobe Photoshop CS5 (Adobe Systems, San Jose, CA, USA) and converted to black and white images by isolating the pixels of the fin rays from the white background. Black and white images were saved and converted into binary files in NIH ImageJ 1.62 (NIH, Bethesda, MD, USA). We then used ImageJ to calculate fin area and the percentage of that area composed of black pixels (fin rays) and white pixels (membrane).

Statistical analysis

We performed Student's *t*-tests to determine if there were significant differences in fin ray flexural stiffness and skeletal area within and across species. Linear regressions were also performed to determine if leading edge flexural stiffness correlates with measurements of fin ray length, body mass and standard body length, and if skeletal area correlates with fin area. The leading edge was chosen for this analysis because the leading edge represents the same fin ray number between species, it is unbranched and branching pattern differs between species, and is the longest fin ray in both species, which suggests its size, and therefore its stiffness, will not be affected by interspecific differences in chord-wise fin shape changes. ANCOVA models were fitted to test for significant differences between the slope and *y*-intercept of the leading edge stiffness by body mass regressions between both species. In the ANCOVA models, stiffness was the dependent variable, species was a factor, and mass was the covariate. All statistical analyses were conducted using the program JMP version 5.0 (JMP 2002) or the R statistical environment (R Development Core Team; www.r-project.org/).

RESULTS

Pectoral fin rays resisted forces of 0.0004–0.4325 N during maximal bending curvatures of 0.2–0.5 mm^{-1}, as fin ray flexural stiffness ranged from 0.0001 to 1.5109 µN m^2. We found similar trends in the fin's span-wise and chord-wise spatial distribution of ray stiffness in *G. varius* and *H. bivitattus* (Fig. 2). Stiffness decreased exponentially along the proximodistal span of a given ray (Table 1). Of the 60 rays examined (four rays per individual) between the two species, 25 of 28 and 24 of 32 showed a significant (P<0.05) exponential relationship between stiffness and proximodistal position in *G. varius* and *H. bivitattus*, respectively (Fig. 3; Table S1). To account for the low number of data points per fin ray and to increase statistical power, within each species, data were pooled by position for each fin ray. An analysis of the pooled data of each fin ray for each species always found a significant (P<0.01) exponential relationship between stiffness and position along the ray's length for a given ray (Table S2). Furthermore, both species showed trends of decreasing ray stiffness along the fin's chord from the leading to trailing edge (Fig. 3; Table 1). The comparison of *y*-intercepts between different regressions can also reveal differences in flexural stiffness between fin rays or species. As no significant difference was detected in the exponential regression slope between any fin ray combinations within a given

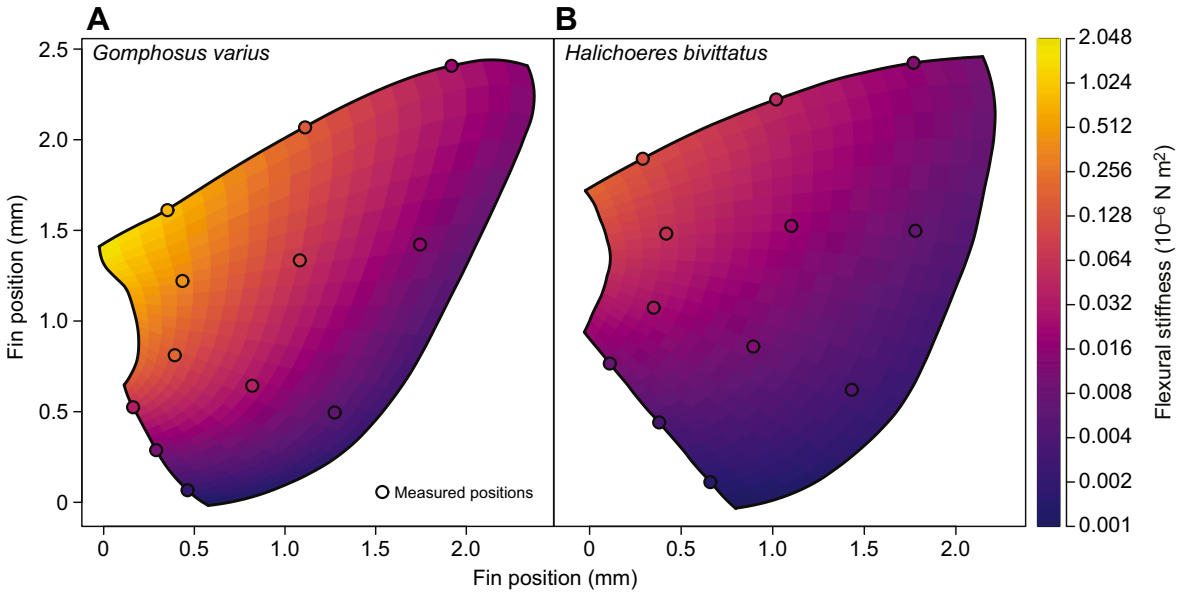

Fig. 2. The average spatial distribution of flexural stiffness across the pectoral fins of *Gomphosus varius* and *Halichoeres bivittatus*. (A) *Gomphosus varius*; (B) *Halichoeres bivittatus*. In both species, flexural stiffness decreased in the span-wise direction and along the chord from the leading to the trailing edge. Flexural stiffness was approximately an order of magnitude greater in *G. varius* in comparison with *H. bivittatus*. Each black circle represents the locations across the fin where three-point bending tests were conducted.

Journal of Experimental Biology (2018) 221, jeb163360. doi:10.1242/jeb.163360

Table 1. Raw data, mean and s.d. of fin ray flexural stiffness for each region of each ray per individual

		LE			M1			M2			TE	
Individual	Proximal	Middle	Distal	Proximal	Middle	Distal	Proximal	Middle	Distal	Proximal	Middle	Distal
Gomphosus varius												
1	1.1701	0.2256	0.0566	0.8054	0.1459	0.0261	0.1832	0.0577	0.0128	0.0709	0.0188	0.0039
2	1.1202	0.1134	0.0197	0.4194	0.1103	0.0220	0.1223	0.0438	0.0137	0.0148	0.0062	0.0032
3	1.5109	0.2159	0.0180	1.1901	0.1733	0.0150	0.3655	0.0161	0.0004	0.1008	0.0178	0.0034
4	1.1550	0.2100	0.0327	0.5434	0.0865	0.0204	0.1829	0.0432	0.0106	0.0524	0.0359	0.0266
5	0.4891	0.1651	0.0166	0.3264	0.1140	0.0333	0.4662	0.0467	0.0072	0.0869	0.0100	0.0001
6	0.4884	0.1108	0.0140	0.3370	0.0653	0.0140	0.1287	0.0362	0.0083	0.0178	0.0049	0.0010
7	0.2956	0.0705	0.0120	0.1474	0.0373	0.0117	0.1018	0.0375	0.0113	0.0099	0.0025	0.0009
Mean	0.8899	0.1588	0.0242	0.5385	0.1047	0.0203	0.2215	0.0402	0.0092	0.0505	0.0137	0.0056
s.d.	0.4587	0.0613	0.0158	0.3532	0.0465	0.0076	0.1393	0.0127	0.0045	0.0371	0.0116	0.0094
t-test *P*-value	**0.0010**	**0.0252**	0.8732	**0.0068**	**0.0335**	0.4457	**0.0254**	**0.0137**	0.1267	**0.0118**	**0.0475**	0.2968
Halichoeres bivittatus												
1	0.0979	0.0337	0.0092	0.0456	0.0095	0.0035	0.0201	0.0083	0.0021	0.0065	0.0031	0.0013
2	0.0308	0.0157	0.0073	0.0120	0.0046	0.0021	0.0065	0.0047	0.0010	0.0064	0.0019	0.0004
3	0.0884	0.0260	0.0060	0.0304	0.0072	0.0022	0.0232	0.0098	0.0026	0.0064	0.0013	0.0004
4	0.0992	0.0493	0.0148	0.0448	0.0194	0.0075	0.0118	0.0096	0.0078	0.0169	0.0081	0.0032
5	0.1264	0.0449	0.0196	0.0683	0.0344	0.0195	0.0393	0.0185	0.0069	0.0040	0.0029	0.0023
6	0.1461	0.0416	0.0044	0.0693	0.0199	0.0044	0.0152	0.0079	0.0044	0.0031	0.0021	0.0015
7	0.2421	0.0791	0.0218	0.2053	0.0412	0.0091	0.1891	0.0389	0.0052	0.0146	0.0081	0.0042
8	0.5058	0.2504	0.1333	0.3966	0.1795	0.0626	0.2458	0.0486	0.0142	0.0299	0.0081	0.0025
Mean	0.1671	0.0676	0.0271	0.1090	0.0395	0.0139	0.0689	0.0183	0.0055	0.0110	0.0045	0.0020
s.d.	0.1496	0.0762	0.0434	0.1304	0.0580	0.0205	0.0934	0.0164	0.0042	0.0091	0.0031	0.0013

P-values in bold are significant. *P*-values are for interspecific comparisons. LE, leading edge ray; M1 and M2, middle fin rays; TE, trailing edge ray.

species (Table S3), differences in the *y*-intercept imply shifts in the magnitude of the exponential relationship between flexural stiffness and fin ray position. Within each species, an analysis of the regressions between stiffness and ray position on the pooled data for each ray revealed significant differences ($P<0.001$) between the *y*-intercepts for the leading and trailing edge as well as middle ray 1 (M1) and the trailing edge (Table S3). For *G. varius*, the leading edge and middle ray 2 (M2) also exhibited a significant difference ($P<0.01$) in the *y*-intercept of a regression between stiffness and the position along the fin ray. These results, together with the lack of significant differences between the *y*-intercepts of adjacent rays, suggest that fin ray stiffness gradually decreases along the fin's chord, from leading to trailing edge, in both species.

A comparison between species reveals significant differences in fin ray stiffness (Fig. 2). For the leading edge, the average flexural stiffness of the proximal and middle portion of the ray was significantly greater ($P<0.05$) in *G. varius* than in *H. bivittatus* (Fig. 3), and averaged 0.8899±0.4587 and 0.1588±0.0613 μN m^2 in *G. varius* and 0.1671±0.1496 and 0.0676±0.0762 μN m^2 in *H. bivittatus* (Table 1). Furthermore, because the stiffness of the fin tip will affect the shedding of wing tip vortices, we assessed how the exponential decrease in pectoral fin ray stiffness has an impact on the comparison of stiffness at the distal tips between species. A comparison of stiffness at the distal tip of the leading edge fin ray between *G. varius* and *H. bivittatus* revealed no significant difference (Table 1; Fig. 4). Similar trends in fin ray stiffness between *G. varius* and *H. bivittatus* were also found for M1, M2 and the trailing edge ray (Table 1). To further test differences in flexural stiffness between species we compared *y*-intercepts of exponential regressions for each fin ray between species. For each fin ray, the *y*-intercept was significantly greater in *G. varius* than in *H. bivittatus* (Table S2).

Fin ray stiffness is correlated with size in both *G. varius* and *H. bivittatus* (Fig. 5). In both species, there was a significant and positive relationship between fin ray stiffness at 50% ray length and total ray length (Table S4). Similarly, there was a significant and positive relationship between stiffness of the leading edge ray at 50% ray length and body mass (Table S4). Furthermore, ANCOVA models were fitted to the *G. varius* and *H. bivittatus* leading edge ray stiffness by body mass regressions. An ANCOVA model where stiffness is modelled as the dependent variable, species as a factor, and mass as the covariate, reveals no significant interaction between mass and species ($P=0.38$, F-value=0.838), which means that the slope of the regression between mass and stiffness are statistically the same between *G. varius* and *H. bivittatus*. A second ANCOVA model found a significant difference in the *y*-intercepts of the leading edge by mass regressions between *G. varius* and *H. bivittatus* ($P=7.52\times10^{-7}$, F-value=87.08), indicating that the factor, species, has a significant effect on stiffness.

A second regression model was run in order to account for the variation in size among individuals. The regression model was between log stiffness and ray position with an effect of log body size, and the model allowed each species and fin ray combination to have their own slope and intercept. The residual stiffness was then plotted as a function of fin ray position for each species and each fin ray (Fig. S2, Table S5). The results were largely consistent with the raw data, and the interspecific differences became more distinct. In one comparison, the distal tip stiffness of fin ray M2 was significantly greater in *G. varius* in comparison with *H. bivittatus* ($P=0.031$), but all other interspecific trends remained the same.

The percentage of total fin ray area occupied by fin ray versus membrane (fin ray area) was also quantified in five individuals of each species (Fig. 6). Fin rays occupied 55.35±8.12 and 37.96±3.50% of the total fin area (Fig. 6C) in *G. varius* and *H. bivittatus*, respectively. A *t*-test revealed that fin ray area was significantly greater in *G. varius* in comparison with *H. bivittatus* ($P<0.01$). There were no significant trends between skeletal area and fin area, which scales with body size, for either species (Fig. 6D).

DISCUSSION

The movement and deformation pattern of pectoral fins have an impact on their hydrodynamic capabilities (Yamamoto et al., 1995; Walker and Westneat, 2000, 2002a,b; Zhu and Shoele, 2008). The

Journal of Experimental Biology (2018) 221, jeb163360. doi:10.1242/jeb.163360

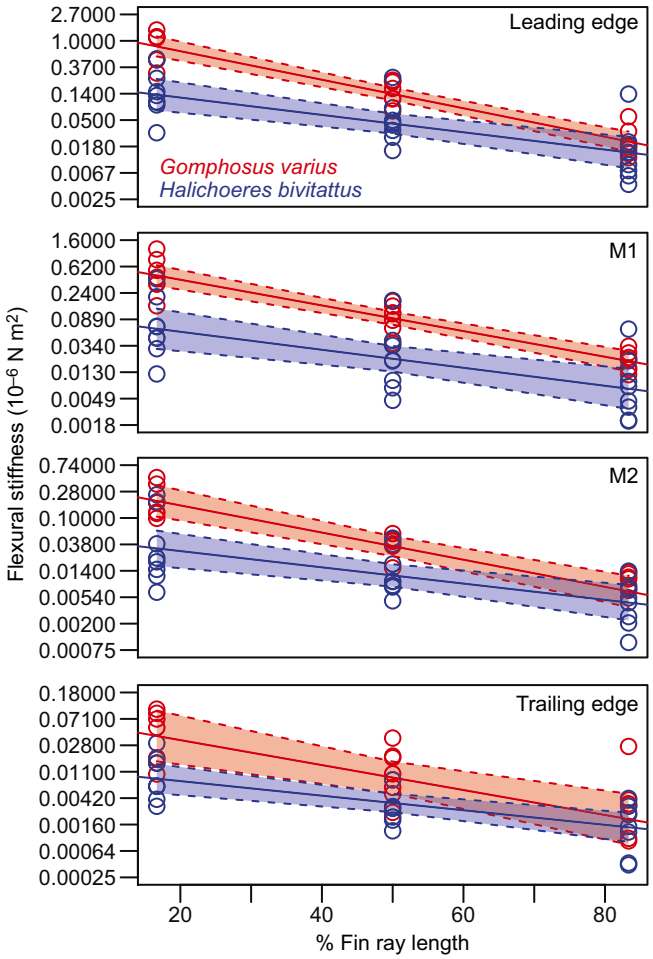

Fig. 3. Flexural stiffness along the length of each fin ray for each species. Flexural stiffness decreased exponentially along the length of each fin ray in the span-wise direction. The *y*-axis of each panel is logarithmically scaled. Significant differences in flexural stiffness of each fin ray at 16.65 and 50.00% fin ray length existed between species. However, there were no significant differences between species in fin ray flexural stiffness at the distal tip (83.34% fin ray length). The red and blue shading represents *G. varius* and *H. bivittatus*, respectively. The shaded region of each fit represents the 99% confidence interval of the linear regression. M1 and M2, middle fin rays.

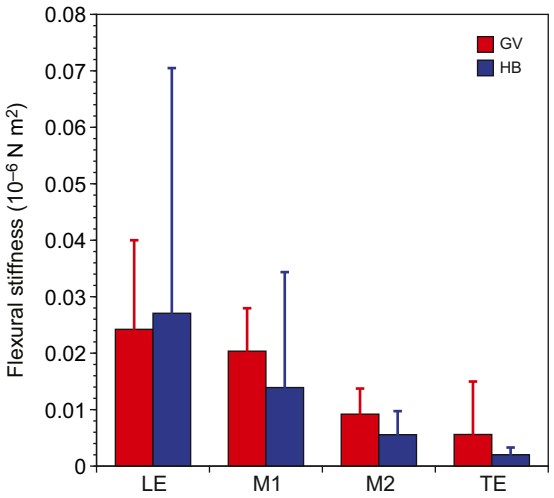

Fig. 4. An interspecific comparison of a fin ray's distal flexural stiffness. In all four fin rays examined, there was no significant difference in a fin ray's distal flexural stiffness (83.34% fin ray length) between species (P>0.05). GV, *G. varius*; HB, *H. bivittatus*; LE, leading edge ray; M1 and M2, middle fin rays; TE, trailing edge ray.

distribution of mechanical properties across fin surfaces will strongly influence fin deformation in response to inertial and hydrodynamic forces during the fin stroke. The purpose of this study was to test our hypotheses by examining the relationship between swimming behavior (e.g. rowing and flapping) and the distribution of flexural stiffness across the pectoral fin (stiffness field). We examined this relationship in two closely related species of wrasse, the flapping *G. varius* and the rowing *H. bivittatus*; the wealth of data published on the ecology, kinematics, motor patterns and hydrodynamic capabilities of these species allows us to better infer the effects of different pectoral fin ray stiffness fields. In both species, fin ray flexural stiffness decreased exponentially along the length of any given fin ray (Figs 2 and 3), and fin ray stiffness decreased along the chord from the leading to trailing edge of each fin (Figs 2 and 3). Fin ray flexural stiffness throughout the proximal 70% of each fin ray was nearly an order of magnitude greater in the flapping *G. varius* than in the rowing *H. bivittatus* (Figs 2 and 3), and these interspecific differences in fin ray stiffness are consistent over a range of body sizes (Fig. 5). Although fin ray stiffness was significantly different between species, the slope of the regression between leading edge flexural stiffness and body mass is similar between species (Fig. 5). Therefore, we suggest that the relationship between body size and fin ray stiffness will scale at a similar rate between species. Furthermore, we examined the relative portion of fin surface area occupied by fin ray skeleton (skeletal area), as opposed to membrane, in both species. We found that skeletal area is significantly greater in *G. varius* than in *H. bivittatus* (Fig. 6). The cumulative effect of distributing fin rays of a given stiffness across a fin is probably that the stiffness of the whole fin exhibits similar trends to the stiffness of the fin rays. We suggest that the whole fin stiffness of fins containing relatively stiff fin rays will be stiffer in comparison with fins containing relatively more flexible fin rays. One morphological impact on whole fin stiffness could be the distribution of the fin skeleton, and our results support this hypothesis. Therefore, we suggest that the distribution of fin skeleton is one variable that probably has an impact on the flexural stiffness of fins, and will be an interesting avenue for future research.

The current study provides new insight into the relationship between fin ray form and function and its relationship to swimming behavior. However, a fin ray is a complex and composite structure that, like many biological materials, has non-linear response properties to deformation. The beam theory equation used in this study is only valid for small displacements where $Y \leq 10\%$ of L, because a material can experience shear as well as bending at larger displacements (Blob and LaBarbera, 2001; Young et al., 2012). The addition of shear at displacements greater than 10% of L will increase the force required to bend the structure a given distance, and therefore increase the effective stiffness of a structure. In this study, each fin ray was deflected exactly 2% of total fin ray length (L=20% fin ray length and fin rays were deflected 10% of that distance). This corresponds to a bending curvature ranging from about 0.2 to 0.5 mm^{-1}. Based on measurements of images of fin bending during flow-tank swimming published for these two species (Walker and Westneat, 2002a,b; Aiello et al., 2017), the fin rays are typically bent into curvatures of about 0.2–0.3 mm^{-1} in the flapping *G. varius* and from 0.2 to 0.5 mm^{-1} in the rowing *H. bivittatus*. The bending tests presented here thus cover a large part of

Journal of Experimental Biology (2018) 221, jeb163360. doi:10.1242/jeb.163360

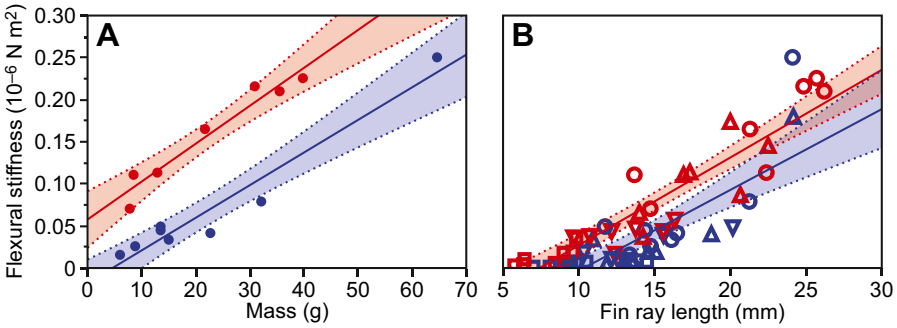

Fig. 5. The relationship between body size and flexural stiffness. (A) Leading edge flexural stiffness at 50% fin ray length is positively and significantly correlated with body mass in both species, and (B) fin ray stiffness is positively and significantly correlated with fin ray length in both species. In both cases there were no significant differences in the regression slope between species. The red and blue shading represents *G. varius* and *H. bivittatus*, respectively. Circles, LE; triangles, M1; upside-down triangles, M2; squares, TE.

the range of natural bending in these structures. However, higher resolution measurements of active fin ray bending across the fin surface during normal and maximal swimming behaviors are needed to more precisely match them up with the bending ranges tested here. Furthermore, the raw force–displacement data (Fig. S1) reveal some degree of elastic non-linearity at larger deformations in this range. For example, fin ray M2 in *G. varius* is slightly stiffer at high displacements in comparison with lower displacements, while M2 in *H. bivattatus* is slightly less stiff at high displacements in comparison with lower displacements (Fig. S1). By integrating individual fin ray stiffness with future work on mechanical properties of the fin membrane that acts primarily in tension, and incorporating non-linear models of fin ray stiffness with increasing fin ray deformation (Alben et al., 2007), we will attain a more complete understanding of the biomechanics of twisting, bending pectoral fins in these high-performance labriform swimmers.

Design principles of a flexible propulsor

Biological propulsors across a variety of systems have convergently evolved a reduction in flexural stiffness along their spans through a structure that tapers, which results in a finer tip than base. Multiple examples of this principle exist in nature. The shafts of bird feathers (Bachmann et al., 2012) and the wings of insects (Combes and Daniel, 2001, 2003b) both decrease in stiffness along their proximodistal span. This can also be seen in the pectoral fins of bluegill sunfish, which employ rays with a proximal portion that is two to six times stiffer in comparison with its distal tip (Tangorra et al., 2010; Lauder et al., 2011). Similarly, this study and previous work on labrid pectoral fin ray stiffness (Aiello et al., 2017) found that fin ray stiffness decreases exponentially along the span of fin rays. In a study using biorobotic pectoral fins, fins with tapered rays had greater propulsive capabilities in comparison with fins outfitted with rays of uniform dimensions (Tangorra et al., 2010). Furthermore, in both engineered and biological systems, the spanwise tapering of a propulsor will increase tip flexibility (Wootton, 1992; Flammang et al., 2013). Increased tip flexibility can then reduce damage from the application of unexpected forces or impacts (Wootton, 1992; Flammang et al., 2013). Together with previous studies on propulsor stiffness in fishes and other systems, our data provide additional mechanical evidence to support hypotheses that animals employing flexible propulsive appendages have convergently evolved structures that decrease in stiffness along their spans.

The highly flexible distal tips of fin rays employed by flappers might also be advantageous for reducing induced drag from wing tip vortices. The flapping swimming behavior utilizes lift-based propulsion that relies on the generation of circulating vortices and dorsoventral pressure gradients (Spedding, 1992; Vogel, 2003). The shedding of vortices from wing tips and local flow from the

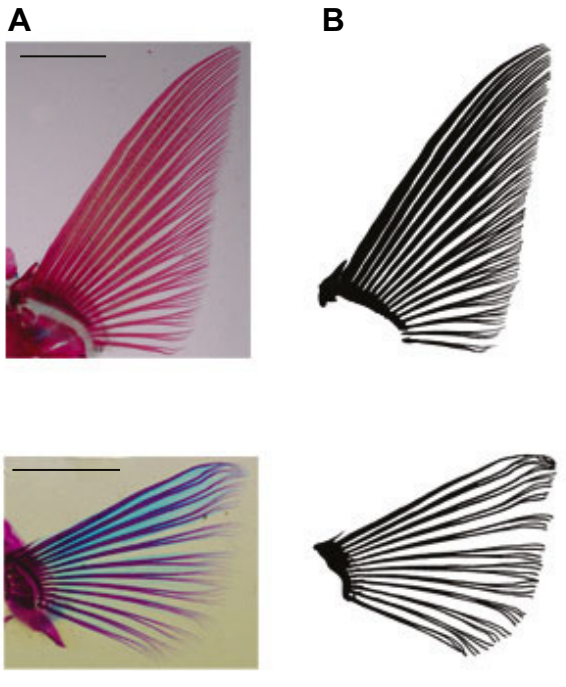

Fig. 6. A comparison of skeletal area between *G. varius* and *H. bivittatus*. Pectoral fins were cleared, stained and photographed (A), and converted into black and white binary images (B) for analysis. Scale bar, 1 cm. Pectoral fin skeletal area (the percentage of the fin area occupied by fin rays versus membrane) was significantly greater in *G. varius* in comparison with *H. bivittatus* (C). There was no significant relationship between fin area and skeletal area in either species (D). *Gomphosus varius* P=0.5487, r^2=0.1315, F-ratio=0.454; *H. bivittatus* P=0.7211, r^2=0.04878, F-ratio=0.1538.

dorsoventral pressure gradient across the wing results in induced drag (Vogel, 2003). However, animals have evolved traits to reduce the magnitude of induced drag caused by the shedding of wing tip vortices. For example, birds have evolved slotted wing tips that reduce induced drag during flight (Tucker, 1993). Similarly, aerodynamic wing theory has been inspired by biology, and engineers have implemented vertically oriented wing tips, also known as winglets, to reduce the shedding of wing tip vortices and reduce induced drag (Hossain et al., 2011). Despite *G. varius* having significantly stiffer fin rays throughout the proximal 66% of each ray in comparison with *H. bivittatus*, there were no significant differences in distal fin ray flexural stiffness between these species (Fig. 4). Flexural stiffness measurements from the third fin ray of three additional flapping labrids (all representing independent evolutions of the flapping behavior) also yields highly flexible distal tips (Aiello et al., 2017), and suggests that highly flexible distal fin ray tips is a common feature that has convergently evolved in lift-based flexible propulsors. We suggest that the reduced flexural stiffness of the distal tips in flapping species will localize and increase spanwise bending within the distal third of fins, which might help reduce induced drag and increase lift-to-drag ratios.

Interspecific differences in the spatial variations in stiffness, or stiffness fields, across the fins will produce different bending regimes during swimming. In both *G. varius* and *H. bivittatus*, flexural stiffness was greatest at the leading edge and decreased posteriorly along the fin chord (Fig. 2). A stiffened leading edge is not unique to fish fins and can be found in other flexible propulsors. For example, insect wings have a stiffened leading edge due to increased vein density in this region (Wootton, 1992), and the shafts of leading edge feathers in bird wings are also stiffer in comparison with more trailing edge feathers (Purslow and Vincent, 1978). A stiffened leading edge is advantageous to resist bending caused by the large inertial and fluid dynamic forces associated with the onset of movement and propulsor reversal between the downstrokes and upstrokes. Furthermore, a propulsor with a stiffened leading edge and a more flexible trailing edge will produce a propeller blade-like twist in response to torsional forces (Wootton, 1981, 1992). Wing twisting is prominent across insect species and is suggested to automatically and passively generate camber across the wing (Ennos, 1988a,b; Wootton, 1992). The generation of camber in a propulsor can increase fluid dynamic efficiency as well as increase the resistance to spanwise bending (Jensen, 1956; Vogel, 1967; Ellington, 1984; Wootton, 1992). The pectoral fins of *G. varius* also experience a propeller-like twist throughout their fin stroke (Walker and Westneat, 1997). The data presented here provide a mechanical basis for this kinematic feature of lift-based labriform locomotion and suggest that the propeller blade-like twist, and therefore camber, of the fin could be generated passively. It is unclear if the stiffness field is a specific adaptation for the passive production of camber or whether this is a fortuitous result of a developmental or phylogenetic constraint. Detailed fin kinematics and deformation patterns in the rower, *H. bivittatus*, will be helpful in discerning how the fin stiffness profile has an impact on fin twisting in this behavior.

The pattern of relative fin ray flexural stiffness across fins is similar between *G. varius* and *H. bivittatus*, but different from that of the bluegill sunfish (*L. macrochirus*). In the bluegill sunfish, the central rays are stiffer than the dorsal and ventral rays (Lauder et al., 2011), leading to a bell-shaped curve of stiffness along the fin chord. While *G. varius* and *H. bivittatus* exclusively employ the pectoral fin lift-based and drag-based swimming behaviors, respectively (Walker and Westneat, 2000, 2002a,b), the bluegill primarily uses its pectoral fins for hovering and low-speed swimming before switching to a body-caudal fin gait (Gibb et al., 1994). Bluegill sunfish also employ both the most dorsal and most ventral fin ray as its leading edge at different points of the fin stroke, which allows them to perform both lift-based and drag-based propulsion (Gibb et al., 1994; Flammang et al., 2013). A study using biorobotic fins found that the spatial distribution of flexural stiffness across a fin could be tuned for directing propulsive forces along different axes (Tangorra et al., 2010). The comparison of the data presented here with that of the bluegill sunfish suggest that the distribution of ray stiffness across the fin could be tuned to interspecific differences in fin movement and loading. Bluegill sunfish have been the primary source of data when designing bioinspired pectoral fin-based propulsors for underwater autonomous vehicles (e.g. Sitorus et al., 2009; Phelan et al., 2010; Tangorra et al., 2011). Data from this study can be used to produce alternative robotic fin shapes and stiffness fields, and informs how the relationship between fin shape and stiffness could be tuned to meet the demands of drag- versus lift-based propulsion (maneuverability versus high-thrust production and efficiency).

The functional morphology of labriform locomotion

The data of this study are drawn from a two-species comparison, yet this work builds upon recent work by Aiello et al. (2017) that compared the flexural stiffness of the third fin ray between a rowing and flapping species in four independently evolving species pairs across the labrid phylogeny. Consistent with this work, our previous study found that, in each independently evolving species pair, flexural stiffness decreases exponentially along the length of the fin ray, and that the fin ray of the flapping species was stiffer in comparison with the rowing species. The aggregated information on the fin ray stiffness field, swimming behavior, hydrodynamic capability and ecology of the Labridae enables us to draw conclusions about fin biomechanics, locomotor behavior and ecology more broadly across the wrasse phylogeny.

Despite performance differences, the evolutionary persistence of the rowing and flapping swimming behaviors, which are the two extremes of the continuum, suggests that these swimming modes are ecologically advantageous (Fish, 1996; Walker and Westneat, 2000, 2002a,b; Wainwright et al., 2002). Indeed, there is a relationship between labrid swimming behavior and habitat use. Flapping species, which achieve high mechanical efficiency (Walker and Westneat, 2000, 2002a,b), generate greater thrust at high speeds, and generally swim at higher cruising speeds in comparison with rowers (Walker and Westneat, 2002a,b; Wainwright et al., 2002) and are typically found at shallower depths away from the reef bottom with greater exposure to high-energy wave-swept environments (Bellwood and Wainwright, 2001; Fulton et al., 2001). Although the relationship between the flexibility and thrust production of a propulsor is complex (Alben, 2008; Ramananarivo et al., 2011; Leftwich et al., 2012; Quinn et al., 2014), in comparison with rigid propulsors (no flexibility), propulsors within a given range of flexibility will typically generate more thrust (Yamamoto et al., 1995; Zhu and Shoele, 2008; Young et al., 2009; Zheng et al., 2013). Yet high degrees of propulsor flexibility can reduce thrust production and propulsive efficiency (Liu and Bose, 1997; Heathcote et al., 2008). Within this window of advantageous propulsor flexibility, Tangorra et al. (2010) showed in a biorobotic pectoral fin model that propulsive forces increase with increasing fin ray stiffness. Our result, that the flapping *G.varius* employs pectoral fins nearly an order of magnitude stiffer than the rowing *H. bivittatus*, suggests that increased fin ray stiffness is a trait that enables the flapper *G. varius* to increase thrust production and

mechanical efficiency in comparison with the rower *H. bivittatus*, a result shown in previous studies (Walker and Westneat, 2000, 2002b). The employment of relatively stiffer fins and associated efficiency and propulsive force production of *G. varius* is advantageous for cruising through high-energy wave-swept coral reef environments.

In contrast to flapping species, rowing species are capable of higher acceleration and thrust production at low speeds, hypothesized to achieve greater maneuverability (Walker and Westneat, 2002a,b; Wainwright et al., 2002), and are typically found at greater depths close to the reef surface with calmer water flow patterns (Bellwood and Wainwright, 2001; Fulton et al., 2001). Fishes are capable of actively controlling the shape and curvature of their fins (Videler, 1977; Geerlink and Videler, 1987; Alben et al., 2007). We suggest that the greater pectoral fin flexibility of the rowing species *H. bivittatus* in comparison with the flapping species *G. varius* will allow *H. bivittatus* to generate three-dimensional fin topographies to maximize its drag coefficient, and have finer control over a wide range of the thrust vectors generated during the power stroke, thus allowing it greater maneuverability. It is not surprising that a rowing species (*H. bivittatus*) employing flexible pectoral fins is found close to the reef bottom where it can take advantage of high accelerations and maneuverability as it traverses the complex substrate to avoid predators and feed. Interspecific variation in fin ray stiffness is thus correlated with interspecific variation in swimming performance in at least these two species, and exemplifies the impact morphological variation can play in driving niche occupation.

Conclusion

Data on the material properties of fin tissues broaden our understanding of fin diversification, and comparison of divergent species highlights the critical role of fin ray stiffness in the transmission of forces externally to the water. In combination with previous comparative work on fin ray flexural stiffness in the Labridae (Aiello et al., 2017), the results presented here show that interspecific differences in pectoral fin flexural stiffness broadly correspond to the behavioral phenotypes of rowing and flapping swimming (Figs 1A and 6A) and provide a correlation between fin mechanics and performance trade-offs in thrust production and maneuverability. Future work should focus on measuring the fin stiffness fields of species using intermediate swimming behaviors as well as rowers and flappers known to be exceptions to the typical habitats occupied by these swimming modes (Bellwood and Wainwright, 2001; Fulton et al., 2001); this future work may reveal additional morphological features that enable fish to maintain both high efficiency and maneuverability. The existence of many extant species employing different degrees of intermediate swimming modes along the rowing–flapping swimming behavior continuum could help shed light on the biomechanical principles of labriform locomotion and the evolutionary dynamics that drive correlated changes in fin shape and mechanical properties.

Acknowledgements

The authors thank Richard Williams IV, Callum Ross, Sliman Bensmaia, Michael LaBarbera, Michael Coates, Hilary Katz, Thomas Stewart, Katharine Henderson and Dallas Krentzel for helpful discussion and/or feedback on the manuscript, and Evan Koch for advice and help with statistical analyses.

Competing interests

The authors declare no competing or financial interests.

Author contributions

Conceptualization: B.R.A., M.E.H., M.W.W.; Methodology: B.R.A., A.R.H., M.E.H., M.W.W.; Formal analysis: B.R.A., C.C., A.M.O., S.R.A., M.W.W.; Investigation: B.R.A.; Data curation: B.R.A., A.R.H., C.C., S.R.A., M.W.W.; Writing - original draft: B.R.A.; Writing - review & editing: B.R.A., A.R.H., A.M.O., S.R.A., M.E.H., M.W.W.; Visualization: A.M.O., S.R.A.; Supervision: B.R.A., M.E.H., M.W.W.; Project administration: M.E.H., M.W.W.; Funding acquisition: M.E.H., M.W.W.

Funding

This work was supported by the National Science Foundation under grants DGE-0903637 (a traineeship that supported B.R.A.), IOS 1425049 and DEB 1541547 (to M.W.W.), and IOS 1257886 (to M.E.H.), and the Office of Naval Research under grant N00014-0910352 (to M.E.H.). Funding also came from The University of Chicago through the Hinds Fund (to B.R.A.).

Supplementary information

Supplementary information available online at
http://jeb.biologists.org/lookup/doi/10.1242/jeb.163360.supplemental

References

Aiello, B. R., Westneat, M. W. and Hale, M. E. (2017). Mechanosensation is evolutionarily tuned to locomotor mechanics. *Proc. Natl. Acad. Sci. USA* **114**, 4459-4464.

Alben, S. (2008). Optimal flexibility of a flapping appendage in an inviscid fluid. *J. Fluid Mech.* **614**, 355-380.

Alben, S., Madden, P. G. and Lauder, G. V. (2007). The mechanics of active fin-shape control in ray-finned fishes. *J. R Soc. Interface* **4**, 243-256.

Bachmann, T., Emmerlich, J., Baumgartner, W., Schneider, J. M. and Wagner, H. (2012). Flexural stiffness of feather shafts: geometry rules over material properties. *J. Exp. Biol.* **215**, 405-415.

Bellwood, D. R. and Wainwright, P. C. (2001). Locomotion in labrid fishes: implications for habitat use and cross-shelf biogeography on the Great Barrier Reef. *Coral Reefs* **20**, 139-150.

Blob, R. W. and LaBarbera, M. (2001). Correlates of variation in deer antler stiffness: age, mineral content, intra-antler location, habitat, and phylogeny. *Biol. J. Linn. Soc.* **74**, 113-120.

Bonser, R. and Purslow, P. (1995). The Young's modulus of feather keratin. *J. Exp. Biol.* **198**, 1029-1033.

Cheney, J. A., Konow, N., Middleton, K. M., Breuer, K. S., Roberts, T. J., Giblin, E. L. and Swartz, S. M. (2014). Membrane muscle function in the compliant wings of bats. *Bioinspir. Biomim.* **9**, 025007.

Combes, S. A. and Daniel, T. L. (2001). Shape, flapping and flexion: wing and fin design for forward flight. *J. Exp. Biol.* **204**, 2073-2085.

Combes, S. A. and Daniel, T. L. (2003a). Flexural stiffness in insect wings. I. Scaling and the influence of wing venation. *J. Exp. Biol.* **206**, 2979-2987.

Combes, S. A. and Daniel, T. L. (2003b). Flexural stiffness in insect wings. II. Spatial distribution and dynamic wing bending. *J. Exp. Biol.* **206**, 2989-2997.

Daniel, T. L. and Combes, S. A. (2002). Flexible wings and fins: bending by inertial or fluid-dynamic forces? *Integr. Comp. Biol.* **42**, 1044-1049.

Ellington, C. P. (1984). The aerodynamics of hovering insect flight. 4. Aerodynamic mechanisms. *Philos. Trans. R. Soc. Lond. B Biol. Sci.* **305**, 79.

Ennos, A. R. (1988a). The importance of torsion in the design of insect wings. *J. Exp. Biol.* **140**, 137-160.

Ennos, A. R. (1988b). The inertial cause of wing rotation in Diptera. *J. Exp. Biol.* **140**, 161-169.

Fish, F. E. (1996). Transitions from drag-based to lift-based propulsion in mammalian swimming. *Am. Zool.* **36**, 628-641.

Flammang, B. E., Alben, S., Madden, P. G. A. and Lauder, G. V. (2013). Functional morphology of the fin rays of teleost fishes. *J. Morphol.* **274**, 1044-1059.

Fulton, C., Bellwood, D. and Wainwright, P. (2001). The relationship between swimming ability and habitat use in wrasses (Labridae). *Marine Biol.* **139**, 25-33.

Geerlink, P. J. and Videler, J. J. (1987). The relation between structure and bending properties of teleost fin rays. *Neth. J. Zool.* **37**, 59-80.

Gibb, A. C., Jayne, B. C. and Lauder, G. V. (1994). Kinematics of pectoral fin locomotion in the bluegill sunfish *Lepomis macrochirus*. *J. Exp. Biol.* **189**, 133-161.

Gillis, G. B. and Blob, R. W. (2001). How muscles accommodate movement in different physical environments: aquatic vs. terrestrial locomotion in vertebrates. *Comp. Biochem. Physiol. A Mol. Integr. Physiol.* **131**, 61-75.

Goodrich, E. S. (1904). On the dermal fin-rays of fishes – living and extinct. *Q. J. Microsc. Sci.* **47**, U465-U18.

Gordon, J. E. (1978). *Structures: or Why Things Don't Fall Down*. New York: Penguin Books.

Heathcote, S., Wang, Z. and Gursul, I. (2008). Effect of spanwise flexibility on flapping wing propulsion. *J. Fluid Struct.* **24**, 183-199.

Higham, T. E., Birn-Jeffery, A. V., Collins, C. E., Hulsey, C. D. and Russell, A. P. (2015). Adaptive simplification and the evolution of gecko locomotion: morphological and biomechanical consequences of losing adhesion. *Proc. Natl. Acad. Sci. USA* **112**, 809-814.

Hossain, A. R. A., Iqbal, A. K. M. P., Ariffin, M. and Mazian, M. (2011). Drag analysis of an aircraft wing model with and without bird feather like winglet. *Int. J. Mech. Aero. Ind. Mech. Manuf. Eng.* **5**, 1894-1899.
Jensen, M. (1956). Biology and physics of locust flight. III. The aerodynamics of locust flight. *Philos. Trans. R. Soc.Lond. B Biol. Sci.* **239**, 511-552.
Kent, G. C. and Carr, R. K. (2001). *Comparative Anatomy of the Vertebrates*. Boston: McGraw Hill.
Lauder, G. V., Madden, P. G., Mittal, R., Dong, H. and Bozkurttas, M. (2006). Locomotion with flexible propulsors: I. Experimental analysis of pectoral fin swimming in sunfish. *Bioinspir. Biomim.* **1**, S25-S34.
Lauder, G. V., Madden, P. G. A., Tangorra, J. L., Anderson, E. and Baker, T. V. (2011). Bioinspiration from fish for smart material design and function. *Smart Mater. Struct.* **20**, 094014.
Leftwich, M. C., Tytell, E. D., Cohen, A. H. and Smits, A. J. (2012). Wake structures behind a swimming robotic lamprey with a passively flexible tail. *J. Exp. Biol.* **215**, 416-425.
Liem, K. F. (1990). Aquatic versus terrestrial feeding modes – possible impacts on the trophic ecology of vertebrates. *Am. Zool.* **30**, 209-221.
Liu, P. and Bose, N. (1997). Propulsive performance from oscillating propulsors with spanwise flexibility. *Proc. R. S. A Math. Phys. Eng. Sci.* **453**, 1763-1770.
Losos, J. B. (1990). Ecomorphology, performance capability, and scaling of West-Indian *Anolis* lizards – an evolutionary analysis. *Ecol. Monogr.* **60**, 369-388.
Lucas, K. N., Johnson, N., Beaulieu, W. T., Cathcart, E., Tirrell, G., Colin, S. P., Gemmell, B. J., Dabiri, J. O. and Costello, J. H. (2014). Bending rules for animal propulsion. *Nat. Commun.* **5**, 3293.
Macleod, G. D. (1980). Mechanical properties of contour feathers. *J. Exp. Biol.* **87**, 65-71.
Mistick, E. A., Mountcastle, A. M. and Combes, S. A. (2016). Wing flexibility improves bumblebee flight stability. *J. Exp. Biol.* **219**, 3384-3390.
Newman, D. J. S. and Wootton, R. J. (1986). An approach to the mechanics of pleating in dragonfly wings. *J. Exp. Biol.* **125**, 361-372.
Phelan, C., Tangorra, J., Lauder, G. and Hale, M. (2010). A biorobotic model of the sunfish pectoral fin for investigations of fin sensorimotor control. *Bioinspir. Biomim.* **5**, 035003.
Purslow, P. P. and Vincent, J. F. V. (1978). Mechanical properties of primary feathers from pigeon. *J. Exp. Biol.* **72**, 251-260.
Quinn, D. B., Lauder, G. V. and Smits, A. J. (2014). Scaling the propulsive performance of heaving flexible panels. *J. Fluid Mech.* **738**, 250-267.
Ramananarivo, S., Godoy-Diana, R. and Thiria, B. (2011). Rather than resonance, flapping wing flyers may play on aerodynamics to improve performance. *Proc. Natl. Acad. Sci. USA* **108**, 5964-5969.
Sitorus, P. E., Nazaruddin, Y. Y., Leksono, E. and Budiyono, A. (2009). Design and implementation of paired pectoral fins: locomotion of labriform fish applied to a fish robot. *J. Bionic Eng.* **6**, 37-45.
Spedding, G. R. (1992). The aerodynamics of flight. *Adv. Comp. Environ. Physiol.* **11**, 51-111.
Steppan, S. J. (2000). Flexural stiffness patterns of butterfly wings (Papilionoidea). *J. Res. Lepid.* **35**, 61-77.
Swartz, S. M. and Middleton, K. M. (2008). Biomechanics of the bat limb skeleton: scaling, material properties and mechanics. *Cells Tissues Organs* **187**, 59-84.
Swartz, S. M., Groves, M. S., Kim, H. D. and Walsh, W. R. (1996). Mechanical properties of bat wing membrane skin. *J. Zool.* **239**, 357-378.
Taft, N. K. (2011). Functional implications of variation in pectoral fin ray morphology between fishes with different patterns of pectoral fin use. *J. Morphol.* **272**, 1144-1152.
Taft, N. K. and Taft, B. N. (2012). Functional implications of morphological specializations among the pectoral fin rays of the benthic longhorn sculpin. *J. Exp. Biol.* **215**, 2703-2710.
Tangorra, J. L., Lauder, G. V., Hunter, I. W., Mittal, R., Madden, P. G. A. and Bozkurttas, M. (2010). The effect of fin ray flexural rigidity on the propulsive forces generated by a biorobotic fish pectoral fin. *J. Exp. Biol.* **213**, 4043-4054.
Tangorra, J. L., Gericke, T. and Lauder, G. V. (2011). Learning from the fins of ray-finned fish for the propulsors of unmanned undersea vehicles. *Mar. Tech. Soc. J.* **45**, 65-73.
Thorsen, D. H. and Westneat, M. W. (2005). Diversity of pectoral fin structure and function in fishes with labriform propulsion. *J. Morphol.* **263**, 133-150.
Tucker, V. A. (1993). Gliding birds - reduction of induced drag by wing tip slots between the primary feathers. *J. Exp. Biol.* **18**, 285-310.
Videler, J. J. (1977). Mechanical properties of fish tail joints. *Fortschr. Zool.* **24**, 183-194.
Vogel, S. (1967). Flight in *Drosophila*. 3. Aerodynamic characteristics of fly wings and wing models. *J. Exp. Biol.* **46**, 431.
Vogel, S. (2003). *Comparative Biomechanics: Life's Physical World.* Princeton, NJ: Princeton University Press.
Wainwright, P. C. and Reilly, S. M. (1994). *Ecological Morphology: Integrative Organismal Biology*. Chicago: University of Chicago Press.
Wainwright, P. C., Bellwood, D. R. and Westneat, M. W. (2002). Ecomorphology of locomotion in labrid fishes. *Environ. Biol. Fishes* **65**, 47-62.
Walker, J. A. and Westneat, M. W. (1997). Labriform propulsion in fishes: kinematics of flapping aquatic flight in the bird wrasse *Gomphosus varius* (Labridae). *J. Exp. Biol.* **200**, 1549-1569.
Walker, J. A. and Westneat, M. W. (2000). Mechanical performance of aquatic rowing and flying. *Proc. R. Soc. B Biol. Sci.* **267**, 1875-1881.
Walker, J. A. and Westneat, M. W. (2002a). Kinematics, dynamics, and energetics of rowing and flapping propulsion in fishes. *Integr. Comp. Biol.* **42**, 1032-1043.
Walker, J. A. and Westneat, M. W. (2002b). Performance limits of labriform propulsion and correlates with fin shape and motion. *J. Exp. Biol.* **205**, 177-187.
Wootton, R. J. (1981). Support and deformability in insect wings. *J. Zool.* **193**, 447-468.
Wootton, R. J. (1992). Functional morphology of insect wings. *Annu. Rev. Entomol.* **37**, 113-140.
Yamamoto, I., Terada, Y., Nagamatu, T. and Imaizumi, Y. (1995). Propulsion system with flexible rigid oscillating fin. *IEEE J. Ocean. Eng.* **20**, 23-30.
Young, J., Walker, S. M., Bomphrey, R. J., Taylor, G. K. and Thomas, A. L. R. (2009). Details of insect wing design and deformation enhance aerodynamic function and flight efficiency. *Science* **325**, 1549-1552.
Young, W. C., Budynas, R. G. and Sadegh, A. (2012). *Roark's Formulas for Stress and Strain*. New York: McGraw-Hill.
Zheng, L. X., Hedrick, T. L. and Mittal, R. (2013). Time-varying wing-twist improves aerodynamic efficiency of forward flight in butterflies. *PLoS ONE* **8**, e53060.
Zhu, Q. and Shoele, K. (2008). Propulsion performance of a skeleton-strengthened fin. *J. Exp. Biol.* **211**, 2087-2100.

Supplementary Information:

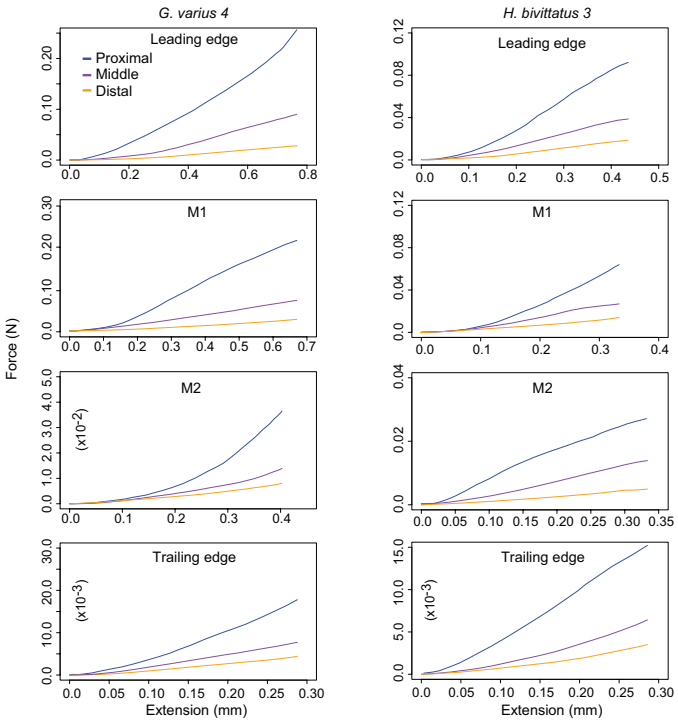

Figure S1. Exemplar plots of force by displacement in each species.
These are plots of force by displacement for one individual (*G.v* 4 and *H.b* 3) of each species. Blue, purple, and orange traces represent measurements from the proximal, middle, and distal location of each fin ray, respectively.

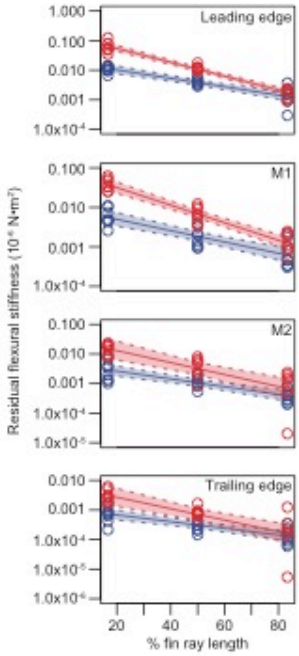

Figure S2. Residual flexural stiffness along the length of each fin ray for each species. Flexural stiffness decreases exponentially along the length of each fin ray in the span-wise direction. The y-axis of each panel is logarithmically scaled. Significant differences in flexural stiffness of each fin ray at 16.65 and 50.00 % fin ray length exist between species. However, in three of four comparisons, there were no significant differences between species in fin ray flexural stiffness at the distal tip (83.34% fin ray length). The red and blue shading represents *G. varius* and *H. bivitattus,* respectively. The shaded region of each fit represents the 99% confidence interval of the linear regression.

Table S1. Exponential regression results for flexural stiffness by fin ray position per individual

Individual	Fin ray	rate	y-intercept	F-value	*P*-value
G. varius 1	LE	-0.045442	0.870682	396.9	0.03193
	M1	-0.0514672	0.643965	16600	0.00156
	M2	-0.039883	-0.974682	175.7	0.04794
	TE	-0.043390	-1.882728	432.8	0.03058
G. varius 2	LE	-0.060604	1.033618	167.1	0.04914
	M1	-0.044211	-0.085760	341.3	0.03443
	M2	-0.032878	-1.530729	768.4	0.02296
	TE	-0.022970	-3.867003	165.7	0.04935
G. varius 3	LE	-0.066482	1.611075	201.5	0.04478
	M1	-0.065613	1.354578	211.8	0.04368
	M2	-0.102649	0.803323	400.0	0.03181
	TE	-0.050679	-1.465586	3964	0.01011
G. varius 4	LE	-0.053479	1.061512	1581	0.01601
	M1	-0.049265	0.146139	211.7	0.04369
	M2	-0.0426729	-0.994213	13870	0.00541
	TE	-0.0101537	-2.793375	222.6	0.04261
G. varius 5	LE	-0.05073	0.33211	23.42	0.1297
	M1	-0.062527	0.206581	275.0	0.03835
	M2	-0.034264	-0.518556	486.7	0.02884
	TE	-0.10567	-0.22733	20.03	0.1399
G. varius 6	LE	-0.053265	0.268485	111.2	0.06019
	M1	-0.0476789	-0.310265	2734	0.01217
	M2	-0.041051	-1.333287	573.1	0.02658
	TE	-0.043153	-3.261613	276.4	0.03825
G. varius 7	LE	-0.048092	-0.360463	266.4	0.03896
	M1	-0.037995	-1.317742	407.3	0.03152
	M2	-0.032931	-1.702513	358.5	0.03359
	TE	-0.035807	-4.071944	138.9	0.05388
H. bivittatus 1	LE	-0.035448	-1.694814	315.3	0.03581
	M1	-0.038302	-2.547252	57.97	0.08314
	M2	-0.034227	-3.249776	57.67	0.08335
	TE	-0.02467	-4.597415	276.9	0.03821
H. bivittatus 2	LE	-0.0215082	-3.106869	859.5	0.02171
	M1	-0.025971	-4.023381	201.8	0.04474
	M2	-0.02811	-4.36824	6.963	0.2306
	TE	-0.041080	-4.312195	212.4	0.04361
H. bivittatus 3	LE	-0.040263	-1.715560	401.8	0.03173
	M1	-0.039437	-2.877594	336.7	0.03466
	M2	-0.032808	-3.139755	68.32	0.07665
	TE	-0.04206	-4.41016	167.5	0.04909
H. bivittatus 4	LE	-0.028554	-1.750345	42.77	0.09659
	M1	-0.026736	-2.641608	807.2	0.0224

	M2	-0.006243	-4.333	42150	0.00099
	TE	-0.025179	-3.626061	192.9	0.04575
H. bivittatus 5	LE	-0.027991	-1.635846	243.8	0.04072
	M1	-0.018791	-2.391191	324.6	0.0353
	M2	-0.026014	-2.764832	177.5	0.04769
	TE	-0.0082143	-5.392597	84.20	0.0691
H. bivittatus 6	LE	-0.05265	-0.87963	37.3	0.1033
	M1	-0.041233	-1.938832	348.5	0.03407
	M2	-0.0186658	-3.889812	972.2	0.02041
	TE	-0.0107425	-5.592737	571.3	0.02662
H. bivittatus 7	LE	-0.036120	-0.788057	605.6	0.02586
	M1	-0.046704	-0.821175	3019	0.01158
	M2	-0.053770	-0.698855	216.4	0.04321
	TE	-0.01883	-3.90073	1091	0.01926
H. bivittatus 8	LE	-0.020005	-0.360266	1002	0.02011
	M1	-0.027700	-0.419597	150.6	0.05177
	M2	-0.042796	-0.754719	161.5	0.04999
	TE	-0.037295	-2.909709	1054	0.01961

All P-values were significant to a level of 0.05.

Table S2. Exponential regression results for flexural stiffness by fin ray position using pooled individual data.

							t-test p-values	
Species	**Fin ray**	**rate**	**y-intercept**	**F-value**	r^2	***p*-value**	**Intercept**	**Slope**
G. varius	LE	-0.054013	0.688145	163.9	0.8906	<0.0001	<0.0001*	0.0105*
H. bivittatus		-0.032817	-1.491423	24.09	0.501	<0.0001		
G. varius	M1	-0.047213	-0.012520	126.5	0.8625	<0.0001	0.000169*	0.13784
H. bivittatus		-0.03311	-2.20758	15.84	0.3921	0.0006		
G. varius	M2	-0.050656	-0.789360	60.44	0.7482	<0.0001	0.00054*	0.04616
H. bivittatus		-0.030329	-2.899930	16.64	0.4048	0.0005		
G. varius	TE	-0.04455	-2.50994	19.57	0.4814	0.0003	0.00852*	0.11920
H. bivittatus		-0.026009	-4.342700	19.73	0.4488	0.0002		

*Significant at the alpha=0.05 with a bonferonni correction: p=0.0125

Table S3. *p*-values for y-intercept and slope t-tests for all possible ray comparisons within each species.

		t-test *p*-values	
Species	**Fin rays**	**Intercept**	**Slope**
G. varius	LE, M1	0.04549844	0.26039751
G. varius	LE, M2	0.00186845	0.6678265
G. varius	LE, TE	<0.0001	0.3913602
G. varius	M1, M2	0.08635674	0.65945345
G. varius	M1, TE	0.00026528	0.80820614
G. varius	M2, TE	0.01606239	0.61344427
H. bivittatus	LE, M1	0.2448897	0.9782997
H. bivittatus	LE, M2	0.01726931	0.80462123
H. bivittatus	LE, TE	<0.0001	0.4477198
H. bivittatus	M1, M2	0.2816453	0.8043744
H. bivittatus	M1, TE	0.0006208	0.48889586
H. bivittatus	M2, TE	0.01036972	0.65026443

Table S4. Linear regression results for leading edge fin ray stiffness at 50% fin ray length by body mass and for fin ray stiffness at 50% fin ray length by fin ray length.

Regression	Species	slope	y-intercept	F-value	r^2	*p*-value
LES x mass	*G. varius*	0.00450	0.05767	77.450	0.9394	0.0003
	H. bivittatus	0.00388	-0.01782	93.078	0.9394	<0.0001
FRS x ray length	*G. varius*	0.01042	-0.077185	147.08	0.8498	<0.0001
	H. bivittatus	0.00960	-0.099248	51.131	0.6302	<0.0001

*Significant at the alpha=0.05 with a bonferonni correction: p=0.025
LES = leading edge stiffness at 50% fin ray length
FRS = fin ray stiffness at 50% fin ray length

Table S5. Residual data, mean and s.d. of fin ray flexural stiffness for each region of each ray per individual.

			LE			M1			M2				TE	
	Indiv.	**Prox.**	**Mid.**	**Distal**	**Prox.**	**Mid.**	**Distal**	**Prox.**	**Mid.**	**Distal**	**Prox.**	**Mid.**	**Distal**
	1	0.0492	0.0094	0.0023	0.0338	0.0061	0.0010	0.0077	0.0024	0.0005	0.0029	0.0007	0.0001
	2	0.1242	0.0125	0.0021	0.0465	0.0122	0.0024	0.0135	0.0048	0.0015	0.0016	0.0006	0.0003
	3	0.0790	0.0112	0.0009	0.0622	0.0090	0.0007	0.0191	0.0008	$2.04x10^{-5}$	0.0052	0.0009	$1.7x10^{-4}$
	4	0.0536	0.0097	0.0015	0.0252	0.0040	0.0009	0.0084	0.0020	0.0004	0.0024	0.0016	0.0012
	5	0.0346	0.0117	0.0011	0.0330	0.0033	0.0005	0.0231	0.0080	0.0023	0.0061	0.0007	$5.37x10^{-6}$
	6	0.0775	0.0175	0.0022	0.0535	0.0103	0.0022	0.0204	0.0057	0.0013	0.0028	0.0008	$1.58x10^{-4}$
	7	0.0505	0.0120	0.0020	0.0251	0.0063	0.0020	0.0173	0.0064	0.0019	0.0017	0.0004	$1.56x10^{-4}$
	AVG	**0.0669**	**0.0120**	**0.0017**	**0.0399**	**0.0073**	**0.0014**	**0.0156**	**0.0043**	**0.0011**	**0.0032**	**0.0008**	**0.0003**
	STDEV	**0.0298**	**0.0026**	**0.0005**	**0.0143**	**0.0033**	**0.0007**	**0.0059**	**0.0026**	**0.0008**	**0.0017**	**0.0003**	**0.0004**
T-test	**P-value**	***0.000146***	***$6.6x10^{-06}$***	0.562579	***$2.0x10^{-05}$***	***0.001396***	0.129821	***0.000245***	***0.006609***	***0.031466***	**0.002540**	**0.008503**	0.287945
	1	0.009532	0.003281	0.000897	0.004436	0.000925	0.000345	0.001957	0.000811	0.000199	0.000632	0.000302	0.000122
	2	0.006601	0.003362	0.001573	0.002574	0.000974	0.000455	0.001384	0.001003	0.000212	0.001371	0.000410	$8.8x10^{-05}$
	3	0.013627	0.003999	0.000930	0.004682	0.001111	0.000337	0.003576	0.001506	0.000401	0.000988	0.000201	$5.9x10^{-05}$
	4	0.010581	0.005256	0.001577	0.004778	0.002069	0.000803	0.001261	0.001023	0.000831	0.001801	0.000864	0.000336
	5	0.013483	0.004783	0.002086	0.007279	0.003663	0.002080	0.004192	0.001971	0.000740	0.000430	0.000310	0.000248
	6	0.009967	0.002835	0.000298	0.004729	0.001359	0.000302	0.001033	0.000536	0.000297	0.000214	0.000145	0.000104
	7	0.012257	0.004002	0.001103	0.010393	0.002086	0.000462	0.009573	0.001969	0.000265	0.000740	0.000408	0.000210
	8	0.014034	0.006946	0.003698	0.011004	0.004979	0.001736	0.006819	0.001348	0.000393	0.000830	0.000224	$6.9x10^{-05}$
	AVG	**0.011260**	**0.004308**	**0.001520**	**0.006234**	**0.002146**	**0.000815**	**0.003724**	**0.001271**	**0.000417**	**0.000876**	**0.000358**	**0.000155**
	STDEV	**0.002565**	**0.001330**	**0.001033**	**0.003036**	**0.001458**	**0.000698**	**0.003069**	**0.000524**	**0.000240**	**0.000511**	**0.000224**	**$9.9x10^{-05}$**

p-values italicized and bolded are significant.